

# Cationic Dimyristoylphosphatidylcholine and Dioleyloxytrimethylammonium Propane Lipid Bilayers: Atomistic Insight for Structure and Dynamics

Wei Zhao,<sup>†</sup> Andrey A. Gurtovenko,<sup>‡</sup> Ilpo Vattulainen,<sup>§</sup> and Mikko Karttunen<sup>\*,†</sup>

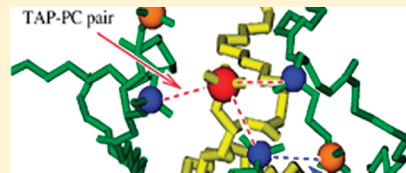
<sup>†</sup>Department of Biological Sciences, University of Calgary, Calgary, Alberta T2N 1N4, Canada

<sup>‡</sup>Institute of Macromolecular Compounds, Russian Academy of Sciences, Bolshoi Prospect 31, V.O., St. Petersburg 199004, Russia

<sup>§</sup>Department of Physics, Tampere University of Technology, P.O. Box 692, FI-33101 Tampere, Finland; Department of Applied Physics, Aalto University School of Science, P.O. Box 11100, FI-00076 Aalto, Finland; and MEMPHYS—Center for Biomembrane Physics, Department of Physics and Chemistry, University of Southern Denmark, Odense, DK-5230 Denmark

<sup>+</sup>Department of Chemistry, University of Waterloo, 200 University Avenue West, Waterloo, Ontario, Canada N6A 5B7

**ABSTRACT:** We performed atomistic molecular dynamics simulations of lipid bilayers consisting of a mixture of cationic dioleyloxytrimethylammonium propane (DOTAP) and zwitterionic dimyristoylphosphatidylcholine (DMPC) lipids at different DOTAP fractions. Our primary focus was the specific effects of unsaturated lipid chains on structural and dynamic properties of mixed cationic bilayers. The bilayer area, as well as the ordering of lipid tails, shows a pronounced nonmonotonic behavior when TAP lipid fraction increases. The minimum in area (maximum in ordering) was observed for a bilayer with TAP fraction of 0.4, that is, at lower TAP fractions compared with saturated PC/TAP bilayers. Adding unsaturated DOTAP lipids into DMPC bilayers was found to promote lipid chain interdigitation and to fluidize lipid bilayers, as seen through enhanced lateral lipid diffusion. The speed-up in lateral diffusion at large DOTAP fractions results from increasing area per lipid, whereas at smaller DOTAP concentrations, the competing effect due to lipid–lipid complex formation results in a constant value for diffusion. We also characterize the lipid headgroup orientation and the interactions between DMPC and DOTAP lipids, which were found to form PC–PC and PC–TAP pairs, and the formation of lipid clusters.



## ■ INTRODUCTION

The development of safe and efficient nanocarriers for drug delivery and gene therapy has attracted great attention.<sup>1,2</sup> In the current arsenal of nanocarriers, cationic liposomes are one of the most promising delivery vectors. They are capable of encapsulating drugs or strands of DNA and delivering them to target regions. In gene delivery, it has been shown that efficiencies of viral transfection vectors are undoubtedly superior to their nonviral counterparts.<sup>3</sup> However, the use of viral vectors is susceptible to triggering immunogenic responses, endangering patients' lives.<sup>4,5</sup> Therefore, nonviral vectors, such as cationic liposomes, are considered more promising and have garnered greater attention.

Cationic liposomes used for delivery often contain at least two kinds of lipid molecules. The key components are cationic lipids. These serve as condensing agents of negatively charged therapeutic molecules, such as antisense oligodeoxynucleotides<sup>6</sup> or DNA strands. Also important are neutral helper lipids, which play a crucial role in determining the structure of the aggregates. Compared with neutral or anionic liposomes, cationic liposomes have distinct advantages because of their overall positive charge, which makes them capable of binding to the negatively charged mammalian cell membranes.<sup>7</sup>

There are several challenges associated with the use of cationic liposomes as efficient drug carriers and transfection vectors. For instance, poor endosomal release of plasmid DNA from

liposome into the cell cytosol and instabilities of liposome/DNA complexes in biological environments are among the major impediments.<sup>1</sup> The former causes low cellular uptake of DNA, and the latter leads to the low delivery rate of DNA from the site of injection to remote target cells. These two impeding factors are determined by the interactions between liposomes and DNA as well as the structural and dynamic properties of liposomes themselves. Their mechanistic elucidation is expected to provide a guideline for rational design of higher efficiency liposome vectors. Despite advances in both *in vivo* and *in vitro* studies on liposome systems,<sup>8,9</sup> a thorough understanding of the nature of atomic-level interactions within the liposome systems is still lacking because of the limits of existing experimental techniques.

A number of molecular dynamics (MD) simulations have been performed to study systems with charged lipids, such as cationic bilayers,<sup>10–12</sup> lipoplexes,<sup>13–15</sup> and micelle fission,<sup>16</sup> by employing all-atom or coarse-grained molecular models. These studies have provided much insight into the electrostatic interactions within the zwitterionic headgroups of helper lipids, the charged headgroups of cationic lipids, and their interactions with counterions and salt, yet the role of hydrocarbon chains in

**Received:** November 4, 2011

**Revised:** November 24, 2011

**Published:** November 25, 2011

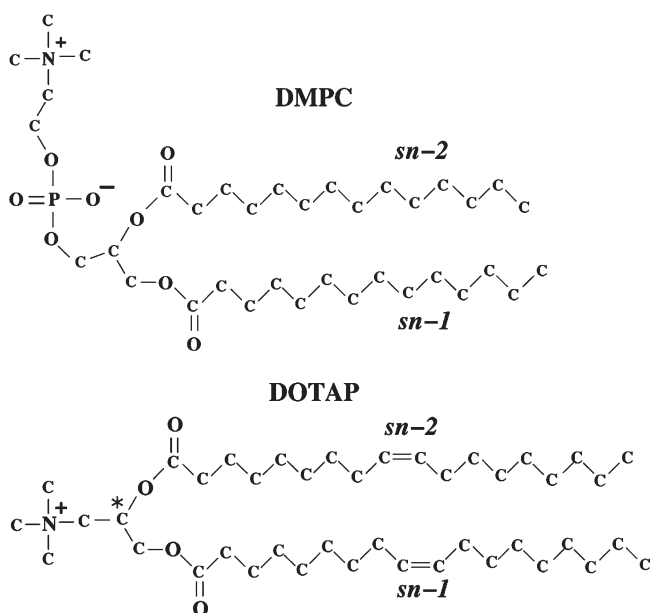


**Figure 1.** Chemical structures of dimyristoylphosphatidylcholine (DMPC) and dioleoyloxytrimethylammonium propane (DOTAP).

determining the structural properties of these liposome systems has not been thoroughly addressed in those simulations. Meanwhile, in experiments, the difference in the acyl chains of the helper and cationic lipids has been found to contribute to the structural properties of cationic liposomes.<sup>17</sup>

Dioleoyloxytrimethylammonium propane (DOTAP; Figure 1) is the most widely used cationic lipid. It has been shown to be efficient both in *in vitro* and *in vivo* applications.<sup>18,19</sup> To the best of our knowledge, the only atomistic MD study involving DOTAP is a 10 ns MD simulation<sup>20</sup> focusing on interactions between amino acids and a DOTAP lipid bilayer of relatively small size (64 lipids). In our study, we prepared mixed cationic dimyristoylphosphatidylcholine (DMPC)/DOTAP bilayer systems in which helper lipids (DMPC; Figure 1) and cationic lipids (DOTAP) differ in their acyl chains. Our major focus is the effects of chain composition on the structural and electrostatic properties of the cationic lipid bilayers. These serve as microscopic models for liposome systems.

Overall, we found that the area per lipid shows a pronounced nonmonotonic behavior when TAP fraction increases, the minimum being located at a TAP fraction of 0.4. Compared with DMPC/DMTAP bilayers, adding unsaturated DOTAP lipids into DMPC bilayers results in lateral expansion and a decrease in the ordering in the hydrocarbon core as well as faster dynamics, as indicated by self-diffusion coefficients of lipids. These changes are also manifested in the dynamic interactions between PC and TAP lipids, which were analyzed in terms of lifetimes of the pairing between PC and TAP headgroups. The consequences of the present findings are discussed at the end of the article.

## ■ MODEL DESCRIPTION AND METHODS

Atomistic MD simulations of hydrated lipid bilayers consisting of mixtures of DOTAP and DMPC lipids were performed using the GROMACS simulation package.<sup>21</sup> We prepared 10 cationic DMPC/DOTAP lipid bilayers with DOTAP fractions of 0.06, 0.16, 0.25, 0.31, 0.39, 0.50, 0.63, 0.75, 0.89, and 1.0. Each of these

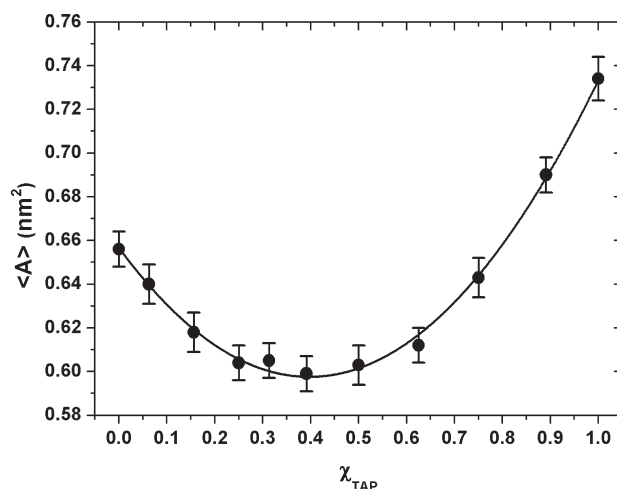


**Figure 2.** Average area per lipid as a function of DOTAP fraction.

bilayers consisted of 128 lipids and  $\sim$ 3600 water molecules. The number of chloride ions matched the number of DOTAPs to ensure charge neutrality. All initial configurations were built up on the basis of an equilibrated hydrated DPPC lipid bilayer.<sup>22</sup> To relax the systems due to structural modifications, energy was first minimized using the steepest descent algorithm. Afterward, a short 10 ps run in the NVT ensemble was performed to eliminate unphysical voids.

The fractional charges within the DOTAP headgroups were taken from our previous study of DMPC/DMTAP bilayers.<sup>10</sup> The force field parametrization of the acyl chains of DOTAP lipid is based on parameters developed previously for DOPC<sup>23</sup> lipids and available at [www.softsimu.org/downloads.shtml](http://www.softsimu.org/downloads.shtml). Force field parameters for the lipids were taken from the united atom force field of Berger,<sup>24</sup> the Ryckaert–Belleman potential<sup>25,26</sup> for hydrocarbon chains, and the OPLS<sup>27</sup> (optimized parameters for liquid simulations) parameters for the Lennard-Jones interactions between united CH groups of acyl chains reparameterized for long hydrocarbon chains to reproduce the experimentally observed values of volume per lipid.<sup>28</sup> The SPC<sup>29</sup> (simple point charge) model was used for water. For chloride ions, we used the default GROMACS force field set, which has been proved to perform well.<sup>30</sup>

A cutoff of 1.0 nm was used for all Lennard-Jones interactions. Bond constraints of lipids and water molecules were handled using the LINCS<sup>31</sup> and SETTLE<sup>32</sup> algorithms, respectively. Electrostatic interactions were computed using the particle-mesh Ewald method,<sup>33–35</sup> and charge groups were ensured to be small to avoid possible artifacts.<sup>36</sup>

The simulations were performed with a time step of 2 fs in the NpT ensemble. The temperature was kept constant at 323 K using the weak coupling thermostat<sup>37</sup> with a coupling time constant of 0.1 ps. Lipids and solvent (water and chloride ions) were coupled separately to a heat bath. The weakly coupled Berendsen barostat,<sup>37</sup> with a coupling constant of 1.0 ps, was applied for pressure control. The pressure coupling was used semi-isotropically such that the height of the box (*z* direction) and the cross sectional area (*xy* plane) were allowed to vary independently of each other.

All simulations were run for 50 ns, which is twice as large as the simulation times of our previous study of DMPC/DMTAP systems.<sup>10</sup> The first 10 ns simulations were used for equilibration,

as monitored by the time evolution of the average area per lipid along with potential energy, temperature and pressure in all systems. The last 40 ns trajectories were used for data analysis. The combined simulation time amounts to 500 ns. In total, the simulations took about 40 000 CPU hours on an AMD Opteron 2.2 GHz CPU. All the error estimates in this study are calculated as standard deviation, unless mentioned otherwise.

## ■ RESULTS

**A. Area Per Lipid.** Area per lipid is one of the most fundamental characteristics of membranes.<sup>38</sup> It is closely related to other physical quantities of membranes, such as ordering of hydrocarbon chains and the dynamics of lipids.

Figure 2 shows the area per lipid for all systems as a function of DOTAP fraction. The average area per lipid ( $\langle A \rangle = 0.656 \pm 0.008 \text{ nm}^2$ ) in a pure DMPC bilayer was taken from our previous study of DMPC/DMTAP bilayers,<sup>10</sup> in which the same force field parameters for DMPC were used. The average area per lipid in a pure DOTAP bilayer was found to be  $0.734 \pm 0.010 \text{ nm}^2$ . This value is larger than the value of  $0.712 \pm 0.007 \text{ nm}^2$  of a pure DMTAP bilayer.<sup>10</sup> The difference of  $\sim 0.02 \text{ nm}^2$  between the area per lipid of DMTAP and DOTAP bilayers is smaller than the difference in area per lipid of  $0.06 \text{ nm}^2$  caused by unsaturation in the acyl chains of PC, as reported by Martinez-Seara et al.<sup>39</sup> We suggest that the high hydration level of cationic TAP headgroups allows introduction of unsaturation without expanding as much as pure PC bilayers do. To our knowledge, experimental measurements of area per lipid in pure DOTAP and DMPC/DOTAP mixtures are still lacking.

Figure 2 shows that the area per lipid behaves nonmonotonically as a function of DOTAP fraction. The minimum of the area per lipid was found to be at the DOTAP fraction of  $\sim 0.4$ . The observed lateral compression of the bilayers at modest amounts of cationic lipids (TAP ratio ranging from 0 to 0.4) is due to closer packing of lipids caused by the reorientation of the dipolar headgroups (P–N) of DMPCs in the presence of DOTAP. Similar observation was also reported in our previous study on DMPC/DMTAP systems.<sup>10</sup> This feature was not captured in a recent coarse-grained simulation work<sup>40</sup> on cationic lipid bilayers, in which the area per lipid was reported to increase exponentially as a function of cationic lipid fraction. This is because the coarse-grained model employed in the aforementioned work did not model the headgroup of the neutral lipid in a sufficiently realistic manner, emphasizing the need for detailed simulations to capture the correct dipolar nature of the headgroup.

In our previous work on DMPC/DMTAP,<sup>10</sup> the minimum was located at a DMTAP fraction of  $\sim 0.5$ , which is in agreement with and confirmed by the experimental data.<sup>41,42</sup> For DMPC/DOTAP bilayers, the position of the minimum is moved to lower TAP fractions and is located at  $\tau_{\text{TAP}} = 0.4$ . The difference is most likely due to a larger volume of the unsaturated acyl chains of DOTAP as compared with DMTAP and to limited compressibility of DOTAP lipids due to double bonds in their acyl chains. This prevents further compression at DOTAP fractions larger than 0.4. This finding is in line with experimental data: in recent experimental measurements,<sup>43</sup> the minimum in the area per lipid of DOPC/DOTAP bilayers was found to be at a cationic lipid fraction of 0.3. Since both cationic and zwitterionic lipids have unsaturated chains in a DOPC/DOTAP bilayer, one can expect that the position of the minimum will be located at smaller  $\tau_{\text{TAP}}$

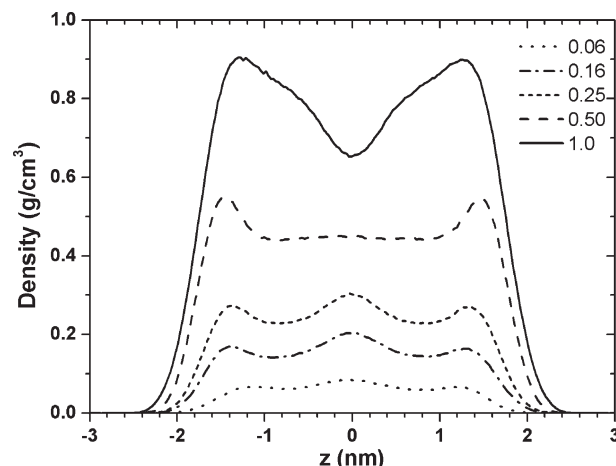


Figure 3. Mass density profiles of DOTAP for all simulated systems.

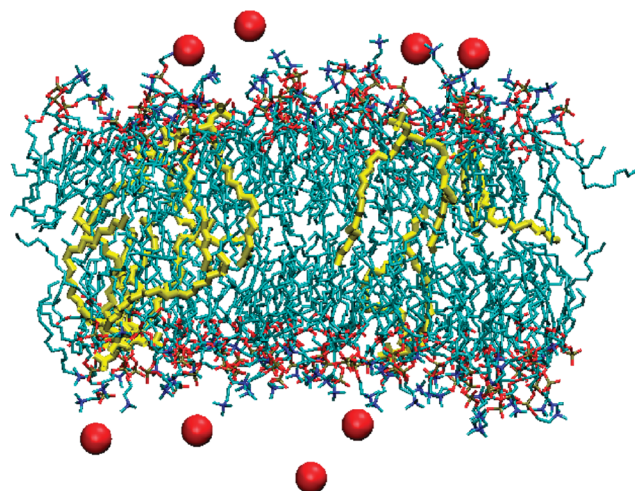
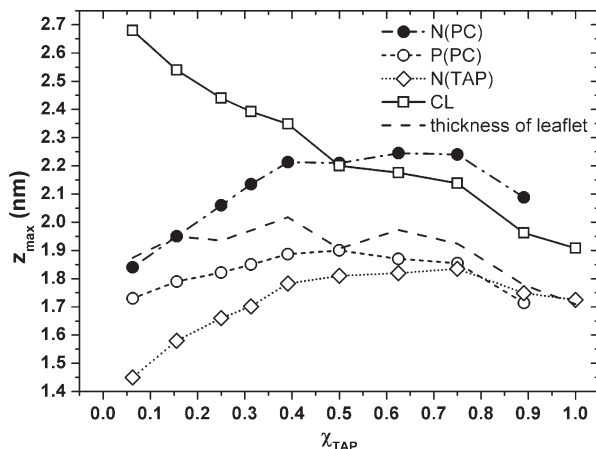


Figure 4. A snapshot of the DMPC/DOTAP lipid bilayer at TAP fraction of 0.06, where DOTAP displays strong interdigitation. DOTAPs are shown in yellow and  $\text{Cl}^-$  ions in red. For clarity, water molecules are not shown.

compared with DMPC/DOTAP bilayers in which only one lipid component is unsaturated. Indeed, the minimum position at  $\tau_{\text{TAP}} = 0.4$  found for DMPC/DOTAP bilayers is between the 0.3 and 0.5 observed for DOPC/DOTAP and DMPC/DMTAP bilayers, respectively.

**B. Density Profiles.** Figure 3 shows the mass density profiles of DOTAPs in all bilayers. As depicted in Figures 3 and 4, DOTAP interdigitates rather strongly across the membrane center. As one can see, this kind of interdigitation is more striking at lower TAP fractions. This is due to the hydrocarbon chains of TAPs that are four carbons longer than those of PCs (from now on, PC refers to DMPC) and the global electrostatics that confines the cationic TAPs deep in the bilayers. Interdigitation becomes weaker at higher TAP concentrations as a result of the repulsive entropic interactions between the two leaflets. At the same time, the interdigitation of PCs becomes weaker as more TAPs are introduced into the bilayers as the total mass density at the bilayer center was found to be well conserved and independent of the TAP fraction (data not shown).



**Figure 5.** Maxima of the density profiles,  $z_{\max}$  for phosphorus and nitrogen atoms from the DMPC headgroups, nitrogen atoms of the DOTAP headgroups, and  $\text{Cl}^-$  ions. The effective thickness of a bilayer leaflet is calculated using the formula:  $d = (1/2) \int (\rho_{\text{lipid}} / (\rho_{\text{lipid}} + \rho_{\text{water}})) dz$  (dashed line).

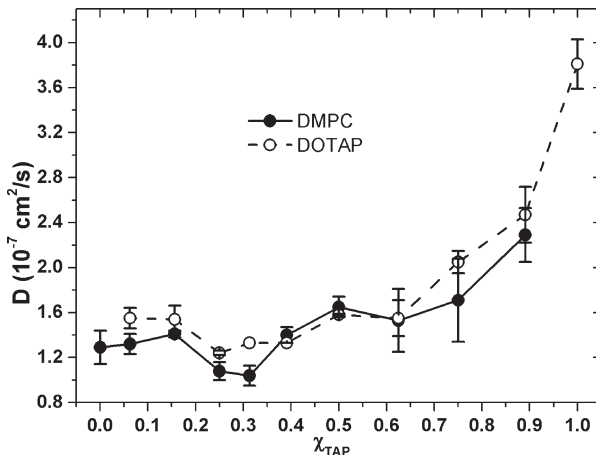


**Figure 6.** Lateral self-diffusion coefficients of DMPC and DOTAP lipids as functions of DOTAP concentration, obtained by fitting the mean squared displacement of each type of lipid with a fitting region from 1 to 4 ns. The errors were given by half the difference between self-diffusion coefficients calculated individually from the  $x$  and  $y$  components of the mean squared displacements.

Figure 5 shows the evolution of the positions of several principal atoms with respect to the center of the lipid bilayers as a function of TAP fraction. One can see that the membrane/water interface, despite some irregularity, moves toward the water phase until the TAP ratio reaches 0.4, that is, the membrane becomes thicker, which is mainly due to the lateral compression of the membrane at modest TAP concentration. Compared with the PC phosphorus atoms, the PC nitrogen atoms show a much stronger increase in their vertical position, indicating reorientation of the PC headgroups. At the same time, the TAP nitrogen atoms also exhibit an increase in vertical position while the chloride ions, on average, move toward the membrane surface. Similar dimensional evolution as a function of the TAP fraction has also been found in DMPC/DMTAP systems; however, the changes in chain composition here (from DMTAP to DOTAP) were found to have negligible effects on the interfacial arrangement of PC and TAP groups.

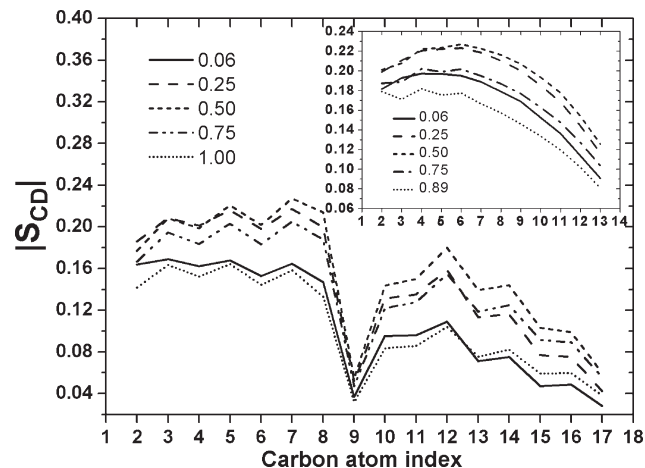


**Figure 7.** Deuterium order parameter  $|S_{CD}|$  averaged over the DOTAP and DMPC (inset) sn-1 and sn-2 chains as a function of DOTAP fraction.

**C. Lateral Diffusion of Lipids.** The lateral diffusion coefficient for each lipid species  $\alpha$  was calculated using

$$D_\alpha = \lim_{t \rightarrow \infty} \frac{1}{4t} \langle r^2(t) \rangle = \lim_{t \rightarrow \infty} \frac{1}{4tN_\alpha} \sum_{i=1}^{N_\alpha} \langle r_i^2(t) \rangle \quad (1)$$

where  $\langle r_i^2(t) \rangle$  is the mean squared lateral displacement of the  $i$ th lipid of lipid species  $\alpha$ , and  $N_\alpha$  is the total number of lipids of type  $\alpha$  in the system. The center of mass movement of each leaflet of the bilayers was removed from the displacements of individual lipids. The results are shown in Figure 6.

The self-diffusion coefficient in pure DMPC bilayer,  $D = 1.29 \pm 0.15 \times 10^{-7} \text{ cm}^2/\text{s}$ , was taken from our previous work. Compared with the DMPC/DMTAP bilayers,<sup>10</sup> DMPC/DOTAP bilayers show much higher mobility for both PC and TAP lipids. For instance, even at a low TAP fraction of 0.06,  $D_{\text{PC}}$  was found to be  $1.07 \times 10^{-7} \text{ cm}^2/\text{s}$  (the values of  $D_{\text{PC}}$  and  $D_{\text{TAP}}$  were taken from ref 10) in the DMPC/DMTAP system, but  $1.31 \times 10^{-7} \text{ cm}^2/\text{s}$  in DMPC/DOTAP, and  $D_{\text{TAP}}$  was found to be  $0.83 \times 10^{-7} \text{ cm}^2/\text{s}$  in the DMPC/DMTAP system and  $1.53 \times 10^{-7} \text{ cm}^2/\text{s}$  in the DMPC/DOTAP system. We can see that the introduction of unsaturated DOTAP tails leads to faster lateral dynamics, which is related to the larger area per lipid and lower ordering (see Section 3D). Our observation confirms the fluidizing effect of DOTAP on membranes reported experimentally.<sup>19,44</sup>

Despite irregularity of self-diffusion coefficients as functions of the TAP concentration, we can see an obvious correlation between the dynamics of lipids with the area per lipid. The lowest lipid mobility was observed for the systems with TAP fractions of 0.25–0.31, which results from bilayer compression and lipid–lipid complex formation. We consider this matter in more detail in the Discussion section. As more TAP lipids were added, the effects of such compression were partially reduced due to the existence of more unsaturated acyl chains, although the largest compression took place at a TAP fraction of 0.4.

**D. Ordering of Lipid Acyl Chains.** The ordering of the lipid acyl chains is usually characterized by the deuterium order parameter,  $S_{CD}$ , measured through  $^2\text{H}$  NMR experiments. The order parameter is defined as

$$S_{CD} = \frac{3}{2} \langle \cos^2 \theta \rangle - \frac{1}{2} \quad (2)$$

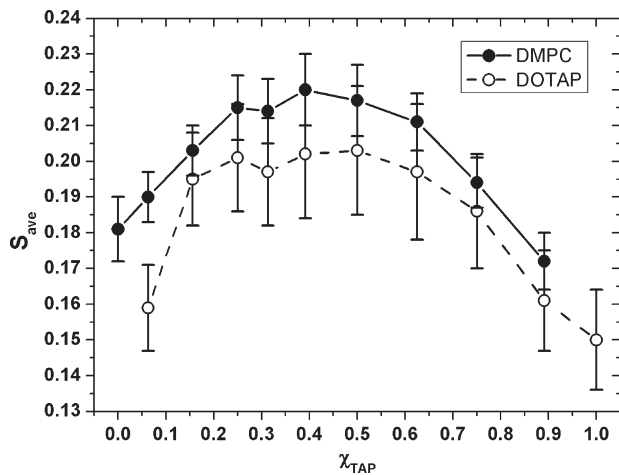


**Figure 8.** Order parameter  $S_{ave}$  calculated by averaging  $S_{CD}$  over C2–C8 hydrocarbons for both DMPC and DOTAP lipids as a function of DOTAP concentration.

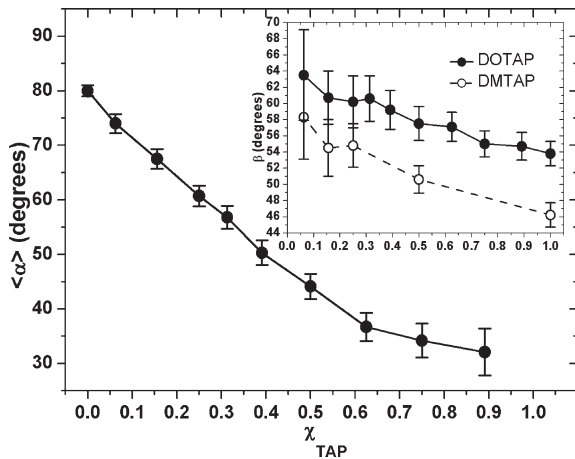


**Figure 9.** The average angle between the P–N vector of DMPC and the bilayer normal, shown as a function of DOTAP fraction. The inset shows the average angle between the C<sup>\*</sup>–N vector of DOTAP and the bilayer normal as a function of DOTAP concentration.

separately for each hydrocarbon group.  $\theta$  is the angle between a CD bond and the bilayer normal.<sup>10</sup>

Figure 7 shows the order parameters of the PC and TAP lipids averaged over their sn-1 and sn-2 acyl chains (see Figure 1). The TAP order parameter is characterized by a slightly rugged plateau between carbons 2 and 8, followed by a highly disordered carbon 9. This disordering results from the existence of the double bond (with regard to carbon atoms 8 and 9). The order parameters of the PC chains also form a plateau between carbons 2 and 8, and they gradually decrease for carbons closer to the ends of the chains.

To characterize the effect of TAP fraction on order parameters of PC/TAP bilayers,  $S_{CD}$  averaged over carbons from 2 to 8 was calculated, as shown in Figure 8. The order parameter is roughly inversely correlated to the area per lipid. As TAP lipids were added, the area per lipid decreased, but the order parameter increased until the TAP fraction reached 0.4, where one can find both the minimum of the area per lipid and the maximum of the order parameter.

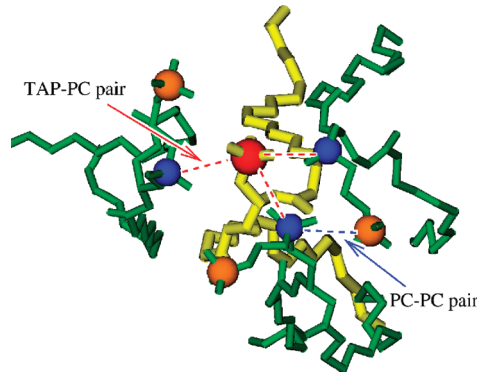


**Figure 10.** Snapshot of TAP forming charge pairs with three PCs. The TAP nitrogen atoms are shown in red; those in PC are shown in orange. The phosphorus atoms are shown in blue.

Compared with DMPC/DMTAP,<sup>10</sup> the  $|S_{CD}|$  values of the acyl chains of DMPC for the DMPC/DOTAP system at the same concentration of cationic lipids are lower throughout the whole chain. This is due to the unsaturated DOTAP hydrocarbon chains with two cis double bonds that disturb the ordering of the hydrocarbon core of the bilayers. This observation confirmed the results reported in our previous study on the effects of unsaturation of neutral lipid bilayers.<sup>39</sup>

**E. Reorientations of PC and TAP Headgroups.** In our previous work on DMPC/DMTAP,<sup>10</sup> we found that the P–N dipoles of PC lipids show pronounced reorientation by pointing upward to the water phase as cationic TAP lipids were added to the bilayer. In the present DMPC/DOTAP systems, similar behaviors were observed. Figure 9 shows the average angle between the P–N dipoles and bilayer normal,  $\langle\alpha\rangle$ , as a function of the TAP concentration. One can see that the P–N dipoles point outward to the water phase as the concentration of TAP fraction is increased. No noticeable differences were found between the PC headgroup orientations in the present DMPC/DOTAP and the previously studied DMPC/DMTAP systems.<sup>10</sup> This suggests that electrostatic interactions dominate headgroup orientation. To the best of our knowledge, no experimental observation is available for comparison. Further NMR measurements could be useful in elucidating the effects of the chain composition on headgroup orientation.

An interesting phenomenon found here is the reorientation of the TAP headgroup represented by the C<sup>\*</sup>–N vector, where C<sup>\*</sup> is the sn-2 carbon (see Figure 1). As shown in the inset of Figure 9, the C<sup>\*</sup>–N vector seems to be suppressed by PCs at low TAP fraction, as indicated by the angle between the C<sup>\*</sup>–N vector and bilayer normal,  $\langle\beta\rangle$ , which was found to be 64° at a TAP fraction of 0.06 and to decrease to 54° in pure DOTAP bilayers. A similar suppression of the TAP headgroup was also revealed by reanalyzing the DMPC/DMTAP systems<sup>11</sup> in the present work. Orientations of the DMTAP and DOTAP headgroups are different at the same TAP concentration. As shown in Figure 9, the orientation angles of the C<sup>\*</sup>–N vector in DMTAP of the corresponding vector in DOTAP are generally 5–8° smaller. The physical origin of this difference is supposedly related to the lesser repulsion between neighboring cationic TAP lipids in DMPC/DOTAP systems, wherein the area per DOTAP is larger because of unsaturation.

**F. Electrostatic Interactions of PC and TAP Headgroups.** To further characterize the PC–PC and PC–TAP interactions,

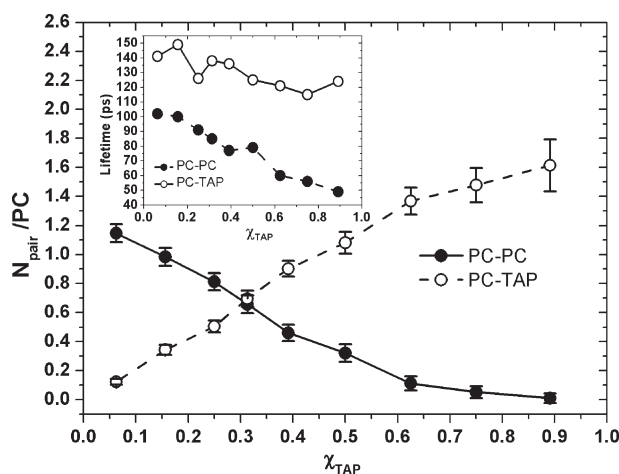


**Figure 11.** Numbers of PC–PC and PC–TAP pairs per PC as functions of DOTAP fraction. The inset shows the lifetimes of PC–PC and PC–TAP pairs as functions of DOTAP concentration.

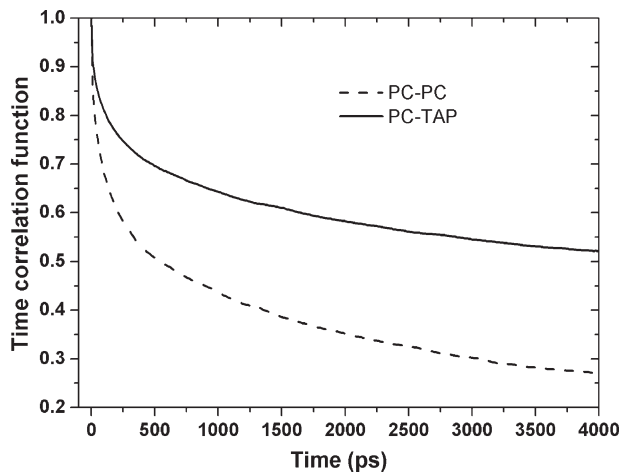


**Figure 12.** Time correlation functions of PC–PC and PC–TAP pairs at a TAP fraction of 0.5.

we considered PC–PC and PC–TAP charge pairs. They are defined here to form if a PC or TAP nitrogen is within the first coordination shell of a PC phosphorus atom<sup>10</sup> (see Figure 10 for illustrations of PC–PC and PC–TAP pairs). In our analysis, a cutoff of 0.67 nm, which is the first minimum of the radial distribution function of PCs with respect to TAPs, was used to define the existence of charge pairs.

Figure 11 shows the average number of PC–PC and PC–TAP charge pairs, defined per PC lipid, as a function of the TAP fraction. We observe that the PC–PC charge pairs are gradually replaced by the PC–TAP charge pairs for increasing TAP concentration. PC–TAP charge pairs are found preferable instead of PC–PC pairs for TAP fractions higher than  $\sim 0.3$ . This is not only due to the decrease in the PC fraction but also because more and more of the P–N vectors reorient themselves toward the water phase for increasing TAP fraction, reducing the ability of PCs to form PC–PC charge pairs. For instance, the average orientation angle of the P–N vectors was found to be  $80 \pm 1^\circ$  in a pure POPC bilayer, decreasing to  $44 \pm 2^\circ$  in a bilayer with a TAP fraction of 0.5 (see Figure 9).

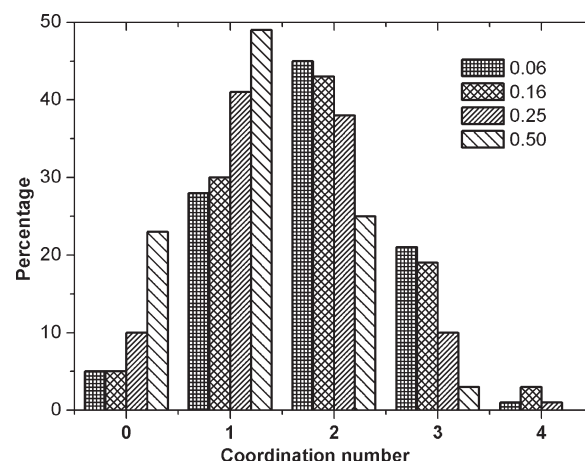


**Figure 13.** Distribution of coordination numbers of PC around TAP at different TAP fractions.

We also measured the average lifetimes of the PC–PC and PC–TAP charge pairs. In our analysis, short breaks of  $\leq 10$  ps were ignored, and pairs with lifetimes  $< 10$  ps were not counted.

The lifetime of the PC–PC charge pairs in pure DMPC,  $103 \pm 289$  ps, is comparable to the value of  $114 \pm 225$  ps of the charge pairing between phosphate oxygen atoms and choline methyl groups in the PC headgroup.<sup>45</sup> The inset in Figure 11 shows that the lifetime of PC–TAP charge pairs (115–149 ps) is longer than that of PC–PC charge pairs (49–102 ps). This is in agreement with the fact that PCs prefer to interact with TAPs. The error bars of the average lifetimes of these pairs are quite large. This is because of the non-Gaussian distribution of the lifetimes, among which the majority are weak and short-lived and a small number of long-lived pairs dominate the global dynamics. For instance, 52% of PC–PC pairs in a pure DMPC bilayer were found to have a lifetime  $\leq 30$  ps. On the other hand,  $\sim 60\%$  of the total pairing time is contributed by PC–PC pairs with lifetimes  $> 200$  ps. The longest observed lifetime of a PC–PC pair was 4.9 ns.

To further illustrate this, we characterize the formation/breaking dynamics using a time correlation function,

$$\begin{aligned} P(t) &= \frac{\langle \delta p(0) \delta p(t) \rangle}{\langle \delta^2 p \rangle} \\ &= \frac{\langle p(0) p(t) \rangle - \langle p \rangle^2}{\langle p \rangle - \langle p \rangle^2} \approx \frac{\langle p(0) p(t) \rangle}{\langle p \rangle} \end{aligned} \quad (3)$$

where the population variable  $p(t)$  is unity when a particular pair (PC–PC or PC–TAP) exists at time  $t$ , and zero otherwise. The angle brackets denote an average over all pairs and all starting times. By definition,  $P(t)$  describes the probability that a particular tagged pair is intact at time  $t$ , given that it was intact at  $t = 0$ .

Figure 12 shows the time correlation functions of PC–PC and PC–TAP pairs in bilayer with a TAP concentration of 0.50. The time correlation function of PC–PC pairs is found to decay much faster than that of PC–TAP pairs, which is in line with the short lifetime of PC–PC pairs. The time correlation functions of both PC–PC and PC–TAP pairs consist of two stages: a very rapid and a slower decay mode. The fast decay indicates temporary formation of pairs that break shortly after, and the slower decay represents reforming and long-lived pairs. Interestingly,

although the time correlation function of PC–TAP pairs decays much more slowly than the one of PC–PC pairs (including the time correlation function of PC–PC pairs in a pure DMPC bilayer), the self-diffusion coefficients of both lipids,  $1.65 \times 10^{-7} \text{ cm}^2/\text{s}$  (DMPC) and  $1.58 \times 10^{-7} \text{ cm}^2/\text{s}$  (DOTAP), are higher than that of DMPC lipids ( $1.29 \times 10^{-7} \text{ cm}^2/\text{s}$ ) in a pure DMPC bilayer. This suggests that the PC–TAP pairs tend to move together.

We also observed the formation of clusters of PC lipids around TAPs, the clusters typically consisting of 2–3 PCs and 1 TAP. Figure 13 shows the distribution of coordination of PCs to TAPs at different TAP fractions. At a TAP concentration of 0.06, 45% of TAPs were found to bind to two PC lipids, and 21% of TAP lipids were found to bind to three PCs (see Figure 10). Clusters consisting of four or more PC lipids were found to be rare.

## ■ DISCUSSION

We have performed atomistic molecular dynamics simulations of mixed bilayers consisting of cationic DOTAP and zwitterionic DMPC lipids. It was found that most structural characteristics of the mixed bilayers demonstrate nonmonotonic behavior with increasing TAP lipid fraction with the minimum observed at TAP fraction equal 0.4. It has been suggested by experiments<sup>46,47</sup> that one key factor in determining the transfection efficiency of cationic liposome is chain unsaturation of lipid components, which could affect the phase transition temperature and the fluidity of the liposomes. This point of view is supported by our measurements on the ordering and dynamic properties. Compared with a DMPC/DMTAP counterpart, the addition of unsaturated DOTAP lipids into DMPC bilayers was found to lead to two major structural effects: two-dimensional expansion (parallel to the bilayer surface) and higher disordering of the hydrocarbon core. Unsaturation of TAPs' acyl chains was also found to result in faster dynamics, which confirmed their fluidizing effects as reported by experiments.<sup>19</sup> We also investigated the dynamic interactions between PC and TAP lipids by analyzing the lifetimes of the pairing between PC and TAP headgroups.

Compared with DMPC/DMTAP bilayers,<sup>10,12</sup> the area per lipid of DMPC/DOTAP bilayers was observed to be larger, which is caused by the unsaturated chains of DOTAP. As a result, the ordering of the nonpolar hydrocarbon tails is also lower as compared with the DMPC/DMTAP systems at the same TAP fractions. Similar effects due to unsaturation of the lipid acyl chains and ordering have been found for zwitterionic lipid bilayers in our previous work.<sup>39</sup> At the same time, the parabolic behavior of the area per lipid indicated bilayer compression at a modest amount of TAPs. However, because of the larger cross-sectional size of DOTAP compared with DMTAP, the TAP ratio at which the DMPC/DOTAP bilayer reaches the smallest possible area is smaller than that in DMPC/DMTAP bilayers.

We observed strong interdigitation of DOTAPs in all mixed DMPC/DOTAP systems. It is expected that the interdigitation would induce a certain degree of transbilayer coupling as well as changes in elastic properties. However, we did not observe interdigitation to slow down the translational diffusion of lipids. This is in agreement with the work by Schram and Thompson, who also found that interdigitation did not influence the translational diffusion of lipids in two model lipid bilayers.<sup>48</sup> Apparently, the area expansion due to unsaturation affects diffusion more than interdigitation.

Compared with anionic lipid bilayers in which neighboring lipids interact with each other via ion (such as sodium) bridges,<sup>49,50</sup> the PC and TAP lipids do not exhibit strong interactions with chloride ions. The most striking finding is that the headgroups of both PCs and TAPs show different orientations at different TAP fractions. Meanwhile, the effects of lipid hydrocarbon chains on the P–N dipoles of the PC lipids were negligible. However, the orientations of the DOTAP headgroups, represented by the C\*–N vector, were observed to differ from those of DMTAP headgroups, which could result from the different tilting angles of the DOTAP and DMTAP chains.

We also studied the electrostatic interactions within the membrane/water interface, mainly focusing on charge pairing between TAPs and PCs, which break and reform dynamically. The lifetimes of PC–TAP pairs were found to be larger than those of PC–PC pairs at all TAP fractions. What is relevant for lateral diffusion is the finding that the lifetimes decrease with increasing DOTAP concentration (Figure 11), suggesting that the lateral diffusion coefficient would increase. However, there is also a competing effect due to decreasing area per lipid for DOTAP concentrations <40 mol % (Figure 2), which tends to slow down diffusion. Together, these effects result in constant diffusion for small DOTAP concentrations. For DOTAP fractions above ~40 mol %, the diffusion speeds up considerably because both increasing area per lipid and decreasing lipid–lipid lifetimes favor this trend.

The data also suggest that the PC–TAP pairs tend to move together, at least up to a few nanoseconds. The PC–TAP pairs also lead to the formation of PC lipid clusters containing two or three PC lipids around TAPs. However, larger clusters consisting of four or more PCs were found rarely, even at low TAP fraction. In particular, this suggests that the analytic model proposed by Levadny and co-workers<sup>51</sup> overestimates the number of PCs around TAPs at low TAP concentration because they assume each TAP lipid to be surrounded by six other PC lipids. In our simulations, at a TAP fraction of 0.06, only 1% of the TAP lipids were found to bind to four lipids. As more TAPs were added, the probability of finding clusters decreased as a result of competition between TAPs. At a TAP fraction of 0.50, 25% of TAPs were found to bind to two PC lipids and only 3% of TAP lipids to bind to three PCs. In our previous study,<sup>11</sup> we found that monovalent ions such as sodium ions could penetrate into the carbonyl regions of DMPC at low concentration of DMTAP lipids, which leads to higher ordering of the acyl chains as well as orientation of the DMPC headgroups. We suggest that similar effects of monovalent ions could also be found in the present DMPC/DOTAP systems.

In our analysis, the effects of unsaturated chains of TAPs on the interactions among the PC and TAP headgroups seem to be negligible. This indicates that electrostatics dominates at the membrane/water interface.

The dependence of elastic properties on the chain composition is also worth investigating for mixed cationic lipid bilayers, since elastic properties are important factors in determining the phase behavior of liposome systems. The interdigitation observed for the DOTAP lipids is supposed to alter the elastic properties of the bilayers. However, the size of systems employed in our study limited us from evaluating membrane elastic behavior. In a recent study by Imparato et al.,<sup>52</sup> MD simulations using a simple coarse-graining model were performed for a mixed bilayer consisting of neutral lipids. They observed that the chain length had an effect on the elastic properties of membranes.

Similarly, further computational studies based on coarse-graining models could possibly reveal the chain length effects on the elastic properties of charged membrane systems.

## AUTHOR INFORMATION

### Corresponding Author

\*Phone: +1-519-888-4567, ext. 31390. E-mail: mikko.karttunen@uwaterloo.ca.

## ACKNOWLEDGMENT

This work has been supported by the Natural Sciences and Engineering Council of Canada (M.K.), the Alberta Heritage Foundation for Medical Research (W.Z.), the Academy of Finland through its Center of Excellence Program (I.V.), the Academy of Finland (I.V. and M.K.), and the Alexander von Humboldt Foundation (A.A.G.). We also thank the Finnish IT Center for Science (CSC), SharcNet ([www.sharcnet.ca](http://www.sharcnet.ca)) and the HorseShoe (DCSC) supercluster facility for computing resources.

## REFERENCES

- (1) Karmali, R. P.; Chaudhuri, A. *Med. Res. Rev.* **2007**, *27*, 696.
- (2) Peer, D.; Karp, J. M.; Hong, S.; Farokhzad, O. C.; Margalit, R.; Langer, R. *Nat. Nanotechnol.* **2007**, *2*, 751.
- (3) Cartier, N.; Hacein-Bey-Abina, S.; Bartholomae, C. C.; Veres, G.; Schmidt, M.; Kutschera, I.; Vidaud, M.; Abel, U.; Dal-Cortivo, L.; Caccavelli, L.; Mahlaoui, N.; Kiermer, V.; Mittelstaedt, D.; Bellesme, C.; Lahlou, N.; Lefrère, F.; Blanche, S.; Audit, M.; Payen, E.; Leboulch, P.; Homme, B.; Bougnères, P.; Von Kalle, C.; Fischer, A.; Cavazzana-Calvo, M.; Aubourg, P. *Science* **2009**, *326*, 818.
- (4) Ledford, H. *Nat. Biotechnol.* **2007**, *25*, 1067.
- (5) Fox, J. L. *Nat. Biotechnol.* **2000**, *18*, 1136.
- (6) Goyal, P.; Goyal, K.; Kumar, S. G. V.; Singh, A.; Katare, O. P.; Mishra, D. N. *Acta Pharm.* **2005**, *55*, 1.
- (7) Koltover, I.; Salditt, T.; Safinya, C. R. *Biophys. J.* **1999**, *77*, 915.
- (8) Katoh, R.; Hara, M.; Tsuzuki, S. *J. Phys. Chem. B* **2008**, *112*, 15426.
- (9) Xu, Y.; Szoka, F. C., Jr. *Biochemistry* **1996**, *35*, 5616.
- (10) Gurtovenko, A. A.; Patra, M.; Karttunen, M.; Vattulainen, I. *Biophys. J.* **2004**, *86*, 3461.
- (11) Gurtovenko, A. A.; Miettinen, M.; Karttunen, M.; Vattulainen, I. *J. Phys. Chem. B* **2005**, *109*, 21126.
- (12) Miettinen, S. M.; Gurtovenko, A. A.; Vattulainen, I.; Karttunen, M. *J. Phys. Chem. B* **2009**, *113*, 9226.
- (13) Bandyopadhyay, S.; Tarek, M.; Klein, M. L. *Phys. Chem. B* **1999**, *103*, 10075.
- (14) Khalid, S.; Bond, P. J.; Holyoake, J.; Hawtin, R. W.; Sansom, M. S. P. *J. R. Soc. Interface* **2008**, *5*, 241.
- (15) Corsi, J.; Hawtin, R. W.; Ces, O.; Attard, G. S.; Khalid, S. *Langmuir* **2010**, *26*, 12119.
- (16) Sammalkorpi, M.; Karttunen, M.; Haataja, M. *J. Am. Chem. Soc.* **2008**, *130*, 17977.
- (17) Kitagawa, S.; Kasamaki, M.; Hyodo, M. *Chem. Pharm. Bull.* **2004**, *52*, 451.
- (18) Campbell, R. B.; Balasubramanian, S. V.; Straubinger, R. M. *J. Pharm. Sci.* **2001**, *90*, 1091.
- (19) Labbe, J.-F.; Cronier, F.; C.-Gaudreault, R.; Auger, M. *Chem. Phys. Lipids* **2009**, *158*, 91.
- (20) Johansson, A. C. V.; Lindahl, E. *J. Chem. Phys.* **2009**, *130*, 185101.
- (21) Lindahl, E.; Hess, B.; van der Spoel, D. *J. Mol. Model.* **2001**, *7*, 306.
- (22) Patra, M.; Salonen, E.; Terama, E.; Vattulainen, I.; Faller, R.; Lee, B. W.; Holopainen, J.; Karttunen, M. *Biophys. J.* **2006**, *90*, 1121.
- (23) Feller, S. E.; Yin, D. X.; Pastor, R. W.; MacKerell, A. D. *Biophys. J.* **1997**, *73*, 2269.
- (24) Berger, O.; Edholm, O.; Jahnig, F. *Biophys. J.* **1997**, *72*, 2002.
- (25) Ryckaert, J. P.; Belleman, A. *Chem. Phys. Lett.* **1975**, *30*, 123.
- (26) Ryckaert, J. P.; Belleman, A. *Chem. Phys. Lett.* **1978**, *66*, 95.
- (27) Jorgensen, W.; Tirado-Rives, J. *J. Am. Chem. Soc.* **1988**, *110*, 1657.
- (28) Nagle, J. F.; Wiener, M. C. *Biochim. Biophys. Acta* **1988**, *942*, 1.
- (29) Berendsen, H. J. C.; Postma, J. P. M.; van Gunsteren, W. F.; Hermans, J. Interaction models for water in relation to protein hydration. *Intermolecular Forces*; Reidel: Dordrecht, 1981; p 331.
- (30) Patra, M.; Karttunen, M. *J. Comput. Chem.* **2004**, *25*, 678.
- (31) Hess, B.; Bekker, H.; Berendsen, H. J. C.; Fraaije, J. G. E. M. *J. Comput. Chem.* **1997**, *18*, 1463.
- (32) Miyamoto, S.; Kollman, P. A. *J. Comput. Chem.* **1992**, *13*, 952.
- (33) Karttunen, M.; Rottler, J.; Vattulainen, I.; Sagui, C. *Curr. Top. Membr.* **2008**, *60*, 49.
- (34) Darden, T.; York, D.; Pedersen, L. *J. Chem. Phys.* **1993**, *98*, 10089.
- (35) Essman, U.; Perela, L.; Berkowitz, M. L.; Darden, H. L.; Pedersen, L. G. *J. Chem. Phys.* **1995**, *103*, 8577.
- (36) Wong-ekkabut, J.; Miettinen, M.; Dias, C.; Karttunen, M. *Nat. Nanotechnol.* **2010**, *5*, 555.
- (37) Berendsen, H. J. C.; Postma, J. P. M.; van Gunsteren, W. F.; DiNola, A.; Haak, J. R. *J. Chem. Phys.* **1984**, *81*, 3684.
- (38) Nagle, J. F.; Tristram-Nagle, S. *Biochim. Biophys. Acta* **2000**, *1469*, 159.
- (39) Martinez-Seara, H.; Rog, T.; Pasenkiewicz-Gierula, M.; Vattulainen, I.; Karttunen, M.; Reigada, R. *J. Phys. Chem. B* **2007**, *111*, 11162.
- (40) Gao, L.; Fang, W. *J. Chem. Phys.* **2010**, *132*, 031102.
- (41) Zantl, R.; Artzner, F.; Sprenger, I.; Rapp, G.; Rädler, J. O. *J. Phys. Chem. B* **1999**, *103*, 10300.
- (42) Olzynska, A.; Jurkiewicz, P.; Hof, M. *J. Fluoresc.* **2008**, *18*, 925.
- (43) Jurkiewicz, P.; Olzynska, A.; Langner, M.; Hof, M. *Langmuir* **2006**, *22*, 8741.
- (44) Cinelli, S.; Onori, G.; Zuzzi, S.; Bordi, F.; Cametti, C.; Sennato, S.; Diociaiuti, M. *J. Phys. Chem. B* **2007**, *111*, 10032.
- (45) Gierula, M. R.; Tokaoka, Y.; Miyagawa, H.; Kitamura, K.; Kusumi, A. *Biophys. J.* **1999**, *76*, 1228.
- (46) Zhi, D.; Zhang, S.; Wang, B.; Zhao, Y.; Yang, B.; Yu, S. *Bioconjugate Chem.* **2010**, *21*, 563.
- (47) Koynova, R.; Tenchov, B. *Soft Matter* **2009**, *5*, 3187.
- (48) Schram, V.; Thompson, T. E. *Biophys. J.* **1995**, *69*, 2517.
- (49) Zhao, W.; Rózsa, T.; Gurtovenko, A.; Karttunen, I. V. M. *Biochimie* **2008**, *90*, 930.
- (50) Zhao, W.; Rózsa, T.; Gurtovenko, A.; Karttunen, I. V. M. *Biophys. J.* **2007**, *92*, 1114.
- (51) Levadny, V.; Yamazaki, C. *Langmuir* **2005**, *21*, 5677.
- (52) Imparato, A.; Shillcock, J. C.; Lipowsky, R. *Europhys. Lett.* **2005**, *69*, 650.